Polarized x-ray-absorption spectra of TiS_2, $TiSe_2$, and $TiTe_2$

S. Bocharov, G. Dräger, and D. Heumann
Fachbereich Physik der Martin-Luther-Universität Halle-Wittenberg, Friedemann-Bach-Platz 6, D-06108 Halle, Germany

A. Šimůnek and O. Šipr
Institute of Physics, Academy of Sciences of the Czech Republic, Cukrovarnická 10, 16200 Praha 6, Czech Republic
(Received 23 March 1998; revised manuscript received 18 May 1998)

We studied the anisotropy of the unoccupied electron states of three titanium dichalcogenides by means of polarized x-ray-absorption spectroscopy. The experimental spectra of TiS_2, $TiSe_2$, and $TiTe_2$ at the Ti K edge and of $TiTe_2$ at the Te L_1 edge were compared with the results of real-space multiple-scattering calculations. The local angular momentum projections of the densities of states at the titanium sites are presented for energies up to 25 eV above the Fermi level. The Ti K-edge spectra of all three dichalcogenides are quite similar to each other provided the differences in their lattice constants are suppressed by comparing the spectra in equivalent energy scales. However, the correspondence between the Te L_1 edge of $TiTe_2$ and the S K edge of TiS_2 is much less pronounced. For most of the spectra good agreement between experiment and theory was found. [S0163-1829(98)01336-8]

I. INTRODUCTION

The titanium dichalcogenides TiS_2, $TiSe_2$, and $TiTe_2$ crystallize in the trigonal space group with one formula unit in the unit cell. Their crystal structure can be considered as a sandwich consisting of chalcogen-Ti-chalcogen slabs. The slabs are internally strongly bonded, but only weakly coupled to each other. This feature allows us to create intercalated sublayers, which could be useful for some technological applications. That is one of the reasons why the electronic structure of titanium dichalcogenides has been the subject of an intensive study lately. The differences between the electronic structure of TiS_2 and $TiSe_2$ were investigated theoretically by Fang, de Groot, and Haas.[1] Photoemission spectroscopy studies were published by Bodicker and Schattke[2] for $TiSe_2$ and by Claessen *et al.*[3] for $TiTe_2$.

For the understanding of this weak bonding mechanism an analysis of the lowest unoccupied electron states can be helpful. Much effort was devoted to x-ray-absorption spectroscopy studies[4–7] of TiS_2 or of Li_xTiS_2 intercalates.[8] However, to our knowledge no published study included a comparison of results for different titanium dichalcogenides, which definitely must correlate with each other and thus prove or negate the adopted conclusions.

In this work we present results of electron state studies by means of the polarized Ti K x-ray-absorption spectroscopy for a range of titanium dichalcogenides (TiS_2, $TiSe_2$, and $TiTe_2$). Because of the site symmetry the lowest unoccupied electron states projected on the Ti atom split into $p_{x,y}$-, p_z-, $d_{xz,yz}$-, d_{xy,x^2-y^2}-, and d_{z^2}-like groups in these compounds. Due to the original experimental technique,[9,10] we were able to separate the spectral components arisen from these different symmetry-resolved groups. The spectral components are considered to reproduce approximately the density of the lowest empty electron states projected on the Ti atom. Saying ''approximately'' we bear in mind effects such as finite initial and final states lifetimes, device smearing, and also the influence of radial transition matrix elements.

II. SPECTRAL ANALYSIS

Here we briefly describe some theoretical foundations of the extracting of symmetry-resolved partial spectral components. We investigate absorption of photons by electrons in solids. Within the one-electron approximation, the absorption coefficient μ can be determined as the probability of electron transition from an initial core state (with wave function ψ_i and energy E_i) to a final unoccupied state (with wave function ψ_f and energy E_f)

$$\mu(\hbar\omega,\mathbf{e},\mathbf{k}) \propto \sum |\langle \psi_f | e^{i\mathbf{k}\cdot\mathbf{r}} \mathbf{e}\cdot\mathbf{r} | \psi_i \rangle|^2 \delta(E_f - E_i - \hbar\omega), \tag{1}$$

where $\hbar\omega$ is the photon energy and $\mathbf{e}$ and $\mathbf{k}$ are the polarization and the wave vectors of the absorbed photon, respectively. The summation involves all initial and final states that have the energy difference of $\hbar\omega$.

In further analysis, we concentrate on the case of K-edge absorption, hence the initial-state wave function ψ_i is $R_0 Y_{00}$. Note that this core wave function is practically nonzero only close to the center of the absorbing atom. The final-state wave function ψ_f can be angularly projected onto the same atom, hence in the region of interest it can be written as a superposition of atomiclike wave functions with definite angular momenta,

$$\psi_f(\mathbf{r}) = \sum_{l,m} R_l(r) Y_{lm}(\hat{\mathbf{r}}). \tag{2}$$

Here $R_l(r)$ and $Y_{lm}(\hat{\mathbf{r}})$ represent radial and angular parts of the wave function, respectively.

In Eq. (1) we consider the first two terms of the expansion $e^{i\mathbf{k}\cdot\mathbf{r}} \approx 1 + i\mathbf{k}\cdot\mathbf{r} + \cdots$, i.e., we take into account electric dipole and quadrupole terms only (other terms do not contribute to x-ray spectra significantly). As the dipole and quadrupole term amplitudes do not interfere, we can rewrite[22] the formula (1)

 © 1998 The American Physical Society

$$\mu(\hbar\omega,\mathbf{e},\mathbf{k}) \propto \delta(E_f - E_i - \hbar\omega) \sum_{l,m}^{} (|\langle R_l Y_{lm}|\mathbf{e}\cdot\mathbf{r}|R_0 Y_{00}\rangle|^2 + \tfrac{1}{4}|\langle R_l Y_{lm}|\mathbf{e}\cdot\mathbf{r}\mathbf{r}\cdot\mathbf{k}|R_0 Y_{00}\rangle|^2). \quad (3)$$

Inserting the mathematical expressions for the angular parts of the wave functions, one can obtain the absorption coefficient as the sum of dipole and quadrupole components $\mu = \mu_D + \mu_Q$, where

$$\begin{aligned} \mu_D &\propto p_x e_x^2 + p_y e_y^2 + p_z e_z^2, \\ \mu_Q &\propto d_{xy}(e_x k_y + e_y k_x)^2 + d_{xz}(e_x k_z + e_z k_x)^2 + d_{yz}(e_y k_z \\ &\quad + e_z k_y)^2 + d_{x^2-y^2}(e_x k_x - e_y k_y)^2 + \sqrt{3} d_{z^2}(e_z k_z)^2. \end{aligned} \quad (4)$$

This means that each polarized spectrum can be interpreted as a weighted sum of partial symmetry-resolved components. Each of the components is formed only by the transitions to orbitals with a definite angle momentum. The factors p_x, p_y, p_z, d_{xy}, d_{xz}, d_{yz}, $d_{x^2-y^2}$, and d_{z^2} represent the so-called partial spectral components, i.e., the densities of states with a definite orbital symmetry modulated by the radial transition probability. We assume the radial matrix elements are equal for all states with equal quantum number l and change with energy only insignificantly. The expressions in parentheses in Eq. (4) (combined from the projections of the vectors **e** and **k** and taken in the power of 2) are the coefficients by these components and are determined just by the actual experimental setting. We call these coefficients partial spectral weights.

Therefore, by measuring three spectra (each of them represented by the absorption coefficient μ) with different orientations I, II, and III of vector **e** relative to the crystal structure, one can use the expression (4) to set up an appropriate system of linear equations and extract the partial-density components p_x, p_y, and p_z:

$$\begin{aligned} \mu^{\mathrm{I}} &\propto p_x (e_x^{\mathrm{I}})^2 + p_y (e_y^{\mathrm{I}})^2 + p_z (e_z^{\mathrm{I}})^2, \\ \mu^{\mathrm{II}} &\propto p_x (e_x^{\mathrm{II}})^2 + p_y (e_y^{\mathrm{II}})^2 + p_z (e_z^{\mathrm{II}})^2, \\ \mu^{\mathrm{III}} &\propto p_x (e_x^{\mathrm{III}})^2 + p_y (e_y^{\mathrm{III}})^2 + p_z (e_z^{\mathrm{III}})^2, \end{aligned} \quad (5)$$

$$\begin{pmatrix} p_x \\ p_y \\ p_z \end{pmatrix} \propto \begin{pmatrix} (e_x^{\mathrm{I}})^2 & (e_y^{\mathrm{I}})^2 & (e_z^{\mathrm{I}})^2 \\ (e_x^{\mathrm{II}})^2 & (e_y^{\mathrm{II}})^2 & (e_z^{\mathrm{II}})^2 \\ (e_x^{\mathrm{III}})^2 & (e_y^{\mathrm{III}})^2 & (e_z^{\mathrm{III}})^2 \end{pmatrix}^{-1} \begin{pmatrix} \mu^{\mathrm{I}} \\ \mu^{\mathrm{II}} \\ \mu^{\mathrm{III}} \end{pmatrix},$$

provided the quadrupole contributions can be neglected. The superscripts in Eq. (5) distinguish between three independent spectra recorded for different sample orientations. In the case of titanium dichalcogenides, the states p_x and p_y are degenerated and the linear system (5) has an order of 2.

Thus, if linearly polarized radiation is absorbed, then in the process of dipole transitions $1s \rightarrow p_{x,y}, p_z$, the partial spectral weights of the two p states will depend on the orientation of the $p_{x,y}$ or p_z orbitals with respect to the polarization vector of the absorbed radiation. In the case of quadrupole transitions $1s \rightarrow d_{xz,yz}, d_{xy,x^2-y^2}, d_{z^2}$, the partial spectral weights will depend on the orientation of the orbitals with respect to the polarization vector and the wave vector as well. The electron transitions described above take into account the symmetry degeneration of electron states, which is equal for all three investigated compounds. As it will follow from Sec. V, it is perfectly justified to neglect all d components here.

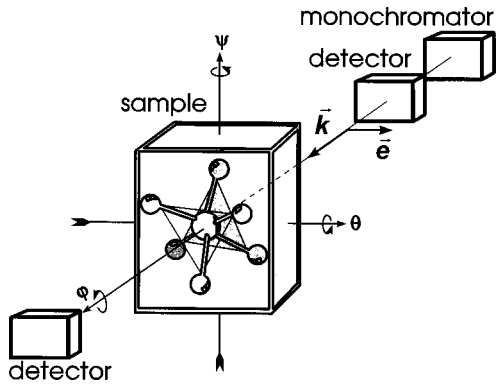

FIG. 1. Scheme of the experimental arrangement. A Ti-chalcogen$_6$ cluster is shown for the (0,0,0) position of the sample.

III. EXPERIMENT

Thin Ti-dichalcogenide plates (TiS_2, $TiSe_2$, and $TiTe_2$) of about $2\times2\times0.02\ \mathrm{mm}^3$ with the trigonal axis oriented perpendicular to the cleavage planes were used as the single-crystal absorption samples. The orientation and crystal quality were verified using the Laue pattern.

The experiments were carried out at the beam line E4 (HASYLAB, Hamburg) equipped with an x-ray focusing mirror and a Si(111) double-crystal monochromator. The sample plates were positioned in a personal computer controlled goniometer allowing three perpendicular rotations φ, θ, and ψ (see Fig. 1) so that any sample orientation with respect to the **e** and **k** vectors of synchrotron radiation can be achieved.

The partial spectral weights of $p_{x,y}$, p_z, and all d components are calculated. As an example their dependence on the angle ψ with $\varphi=0$ and $\theta=0$ is presented in Fig. 2. Our goniometer construction makes the rotation ψ as independent one, the rotation θ dependent on ψ (the θ axis turns by a rotation about ψ), and the rotation φ dependent on ψ and θ.

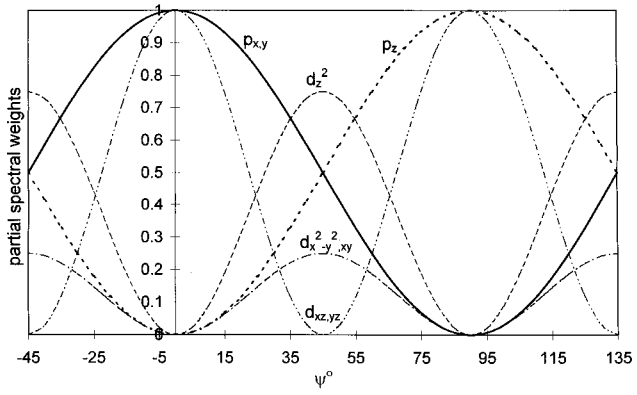

FIG. 2. Partial spectral weights of different Ti p and d orbitals in the K absorption process depending on the rotation angle $\psi°$ of the trigonal crystal structure around the ψ axis (see Fig. 1) for $\varphi=\theta=0$.

TABLE I. Weight coefficients in the absorption process of all symmetry-resolved orbitals for different sample orientations.

Sample position	$p_{x,y}$	p_z	$d_{xz,yz}$	d_{xy,x^2-y^2}	d_{z^2}
$\varphi=0,\ \theta=0,\ \psi=0$	1	0	1	0	0
$\varphi=0,\ \theta=45,\ \psi=0$	1	0	0.5	0.5	0
$\varphi=0,\ \theta=0,\ \psi=45$	0.5	0.5	0	0.25	0.75
$\varphi=0,\ \theta=0,\ \psi=22.5$	0.854	0.146	0.5	0.125	0.375
$\varphi=0,\ \theta=36,\ \psi=29$	0.846	0.154	0.346	0.423	0.231
$\varphi=0,\ \theta=32.7,\ \psi=32.7$	0.793	0.207	0.294	0.396	0.310
$\varphi=0,\ \theta=0,\ \psi=30$	0.75	0.25	0.25	0.188	0.562

In the zero position ($\varphi=0,\ \theta=0,\ \psi=0$) the threefold axis of the trigonal crystal structure coincides with the x-ray beam direction **k**. All spectra were normalized on the equivalent effective sample thickness.

In order to separate the absorption resulting from *K* transitions exclusively, we used a background subtraction. The background function $f(E)=a/E^4+b/E^3+c$ after Victoreen shows acceptable results.

IV. THEORY

Polarized Ti *K*-edge x-ray absorption near-edge structure (XANES) spectra of TiS_2, $TiSe_2$, and $TiTe_2$ as well as polarized Te L_1-edge XANES of $TiTe_2$ were calculated employing the real-space–multiple-scattering (RS-MS) formalism.[11] We used a modified ICXANES computer code of Vvedensky, Saldin, and Pendry.[12] The calculations presented here were performed for clusters of 135 atoms for the Ti edges and of 138 atoms for the Te edge, implying that the radii of these clusters varied between 8.3 and 9.6 Å according to the compound and/or selected edge. Exploratory XANES calculations for a whole series of smaller cluster sizes were performed to verify that a convergence with respect to the number of included atoms had been achieved.[7]

The largest angular momentum included in the single-site scattering was $L_{\max}=4$. Test calculations for all four edges with $L_{\max}$ as large as 6 were done for clusters of 25 atoms with hardly any difference visible.

Non-self-consistent muffin-tin potentials were generated via the so-called Mattheiss prescription (superposition of charge densities of isolated atoms). An energy-independent X_α exchange-correlation potential with the Kohn-Sham value of $\alpha=2/3$ was used.[13] Structural data for TiS_2, $TiSe_2$, and $TiTe_2$ were taken from the CRYSTIN database.[14]

Muffin-tin radii of nonoverlapping spheres were determined so that the ''matching potential condition'' is satisfied. The muffin-tin zero was set to the average interstitial potential. We verified for the particular case of the TiS_2 spectrum that identifying the muffin-tin zero with the value of the inner-sphere potential at the boundaries of muffin-tin spheres (minimizing thus the step in the potential, as suggested, e.g., in Ref. 15) does not change the results significantly even close the absorption edge. Hence we believe that the results presented here are sufficiently robust with respect to the technical details of muffin-tin potential construction (note that the opposite case would point to the unsuitability of the muffin-tin approximation itself).

The influence of the core hole left by the excited electron was taken into account while calculating atomic charge densities by removing one electron from the core level and putting it into the lowest unoccupied atomic level (''relaxed and screened approximation''; see Ref. 16 for a more detailed analysis). Again, for TiS_2 we checked that there was practically no difference between our XANES spectra calculated with and without a core hole.

Theoretical results presented in this paper include broadening by an energy-dependent Lorentzian of full width at half maximum $w=w_0+0.10(E-E_F)$. The constant part w_c accounts for the core hole lifetime and is 0.94 and 3.32 eV for the Ti *K* edge and the Te L_1 edge, respectively.[17] The energy-dependent term represents inelastic energy losses of the photoelectron of energy *E* (the ''Fermi energy'' E_F is identified with the onset of a prepeak for our purpose). This simple ansatz formula proved to be efficient both in metallic[18] and in nonmetallic[19] materials. We will return to the question of inelastic energy losses in Sec. VI.

V. RESULTS

To study the contribution of Ti $1s\rightarrow d$ transitions, we performed several measurements in such experimental settings in which the dipole contributions to the spectra (determined by their partial spectral weights) were always the same, while the quadrupole contributions varied.[9] The differences between spectra recorded for these sample orientations (see, for example, the first two orientations in Table I) did not exceed the experimental error limits of about 1% of the total intensity. Therefore, we suppose that the contribution of Ti $1s\rightarrow d$ transitions is too small to be detected with the available equipment in all three investigated compounds. With this assumption we interpret the spectra as a composition of merely the Ti $1s\rightarrow p_{x,y}$ and $1s\rightarrow p_z$ absorptions. If the assumption is not valid then extraction procedures according to the relation (5) performed for different combinations of spectra will provide inconsistent curves of partial components $p_{x,y}$ or p_z. On the other hand, the coincidence of all curves in the groups $p_{x,y}$ and p_z can serve as a criterion of the reliability of the technique as well as of the validity of the simplifications and assumptions used. The partial spectral weights in the absorption process for $p_{x,y}$, p_z, $d_{xz,yz}$, d_{xy,x^2-y^2}, and d_{z^2} are displayed in Table I for all sample orientations used in the experiments.

The results of the TiS_2 analysis show rather good consistency. Four spectra by different sample orientations were measured and are displayed in Fig. 3(a).

In Fig. 3(b) we present the partial spectral components

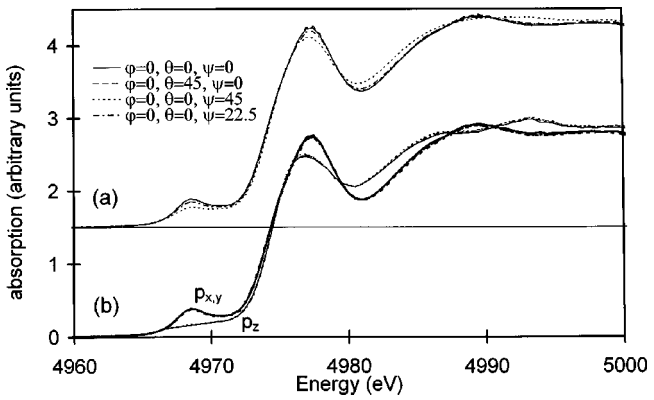

FIG. 3. (a) Polarized Ti K absorption spectra of TiS_2 recorded for four different sample orientations, together with (b) the partial spectral components extracted from three different alternative sets of the experimental spectra. In the ''zero position'' ($\varphi=\theta=\psi=0$) the trigonal axis c coincides with the wave vector **k** and the axis a is parallel to the polarization vector **e** (see Fig. 1).

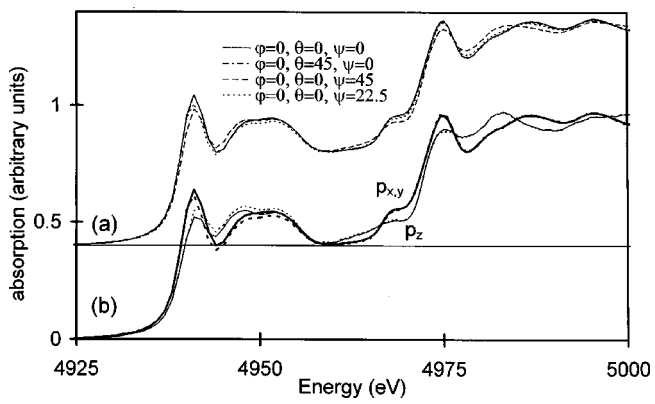

FIG. 5. (a) Polarized Te L_1 and Ti K absorption spectra of $TiTe_2$ recorded for four different sample orientations, together with (b) the partial spectral components extracted from two alternative sets of the experimental spectra. The zero position of the sample is defined as for TiS_2. The Te L_1 absorption begins at about 4930 eV, while the Ti K absorption begins at 4960 eV approximately.

$p_{x,y}$ and p_z extracted from three independent sets of spectra measured at different sample orientations. The equivalent curves obtained from the alternative sets are displayed all together in order to emphasize the reproductivity of the technique.

Analogously to TiS_2, five different Ti K absorption spectra were recorded for $TiSe_2$ [Fig. 4(a)]. The resulting $p_{x,y}$ and p_z components are very similar with those of TiS_2. The only difference is that a better sample quality allowed us to perform one more additional independent measurement and thus to reach a better statistics. In order to compensate for the influence of thickness effects, we applied such sample orientations that provide equal or similar effective sample thicknesses. The curves of the $p_{x,y}$ or p_z components, extracted from alternative combinations of experimental data, coincide perfectly with each other [Fig. 4(b)].

$TiTe_2$ offers a more complicated situation. Here the Te L_1 absorption edge lies very close to that of the Ti K absorption. Nevertheless, the Te L_1 absorption must be predominantly formed by the dipole transitions $2s \rightarrow p$. From the trigonal surrounding of the Te atom one can expect a similar polarization dependence as for Ti K absorption. Therefore, the extraction of partial components from the common spectrum involving both the Te L_1 and the Ti K absorption edges will provide the summarized components Ti $p_{x,y}$+Te $p_{x,y}$ and Ti p_z+Te p_z. The absorption edges are situated so that the Ti K absorption begins at about 4960 eV where the XANES of the Te L_1 absorption is nearly over [see Fig. 5(a)]. In Fig. 5(b) we present the partial spectral components extracted from the common Te L_1 and Ti K absorption spectra of $TiTe_2$.

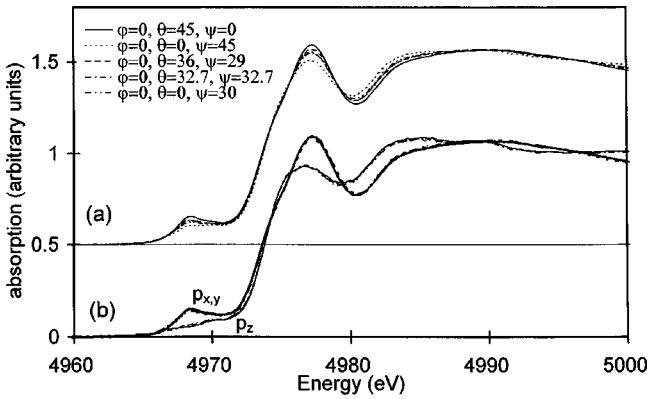

FIG. 4. (a) Polarized Ti K absorption spectra of $TiSe_2$ recorded for five different sample orientations, together with (b) the partial spectral components extracted from four alternative sets of the experimental spectra. The zero position is defined as for TiS_2.

All the investigated compounds have nearly identical geometrical structures; they differ just by a uniform bond-length scaling. Hence, in comparing spectra of TiS_2, $TiSe_2$, and $TiTe_2$, one can make use of the fact that interatomic distances R_{ij} enter the XANES formula only in combination with energy E measured from the muffin-tin zero V_{MTZ}, viz., as arguments in free-electron propagators $\sqrt{E-V_{\mathrm{MTZ}}}R_{ij}$.[11] That means that if XANES spectra in consideration are scaled appropriately, any differences due to different lattice constants will be removed: One can immediately see that if two particular spectral features occur at energies E_1 and E_1' for one compound and at energies E_2 and E_2' for another compound, then neglecting differences in phase shifts one gets

$$(E_1-E_1')R_1^2=(E_2-E_2')R_2^2, \tag{6}$$

where R_1 and R_2 are characteristic interatomic distances in the first and in the second compound, respectively. Any deviations still remaining after such a scaling can be attributed to differences in phase shifts, i.e., in the electronic structure.

In Table II nearest-neighbor distances and corresponding scaling factors according to the relation (6) are presented (we

TABLE II. Scaling factors leading to equivalent energy ranges.

Compound	Nearest-neighbor distance (Å)	Scaling factor
TiS_2	2.42	1.000
$TiSe_2$	2.53	0.915
$TiTe_2$	2.73	0.786

choose a unity scaling factor for TiS_2 by definition). These scaling factors were employed to determine equivalent energy ranges used for displaying experimental as well as theoretical results for TiS_2, $TiSe_2$, and $TiTe_2$ Ti *K*-edge spectra in Fig. 6. The positioning of theoretical spectra in the absolute photon energy scale was set by convenience for each edge, so that the best agreement with corresponding experimental curves is achieved.

In Fig. 6(c) the theoretical Ti *K* edge of $TiTe_2$ is superposed onto the Te L_1 EXAFS (see below). It barely differs from a ''pure'' Ti *K* edge; therefore, a separate Ti *K*-edge calculation is not presented here. The only feature introduced by the presence of the Te L_1 edge is the occurrence of the low-energy tail below the prepeak in the p_z component (around $E=4962$ eV). For all three compounds, a full convergence of the calculation with respect to cluster sizes was achieved at 99 atoms; however, gross features of the full-cluster theoretical spectra were reproduced for 51 atoms already.

Experimental and theoretical Te L_1-edge polarized spectra of $TiTe_2$ are compared in Fig. 7, together with analogous data for the S *K* edge of TiS_2 taken from the literature.[5,7] Note that both of these spectra probe unoccupied *p* states as ''seen'' from the anion site. Again, energy ranges of the plots were scaled according to Table II. As the experimental and theoretical S *K*-edge spectra of Ref. 5 are not polarized, we included in Fig. 7 also calculated projected densities of unoccupied states published by Šimůnek *et al.*[7]

The onset of the Ti *K* edge is shown in the figure as well. The energy separation between the theoretical Ti and Te edges (27 eV) was taken over from the measured spectra, while the ratio between the calculated intensities of the Te and Ti edges was provided by the theory itself.

The two main peaks at 4941 and 4950 eV can be reproduced (with a correct polarization dependence) for a cluster containing 16 atoms. On the other hand, even 57 atoms was not enough to generate the second peak splitting, which appears only for yet larger clusters.

VI. DISCUSSION

Titanium dichalcogenides TiS_2, $TiSe_2$, and $TiTe_2$ show a very similar behavior with respect to the process of the polarized x-ray absorption. There is an apparent correlation between spectral features of the three compounds and nearly each qualitative conclusion is valid in all three cases simultaneously. In particular the energy separation between the prepeaks and the main peaks as well as between the main peaks and the second peaks are roughly identical for all three compounds, provided the energy scaling according to Eq. (6) is taken into account (see Fig. 6).

The real-space multiple-scattering calculation reproduces the measured spectra quite well both in peak positions and in polarization dependence. For TiS_2, it compares better than the calculations of Antonangeli *et al.*[4] This contradiction is a bit surprising, given the fact that Antonangeli *et al.* use a method similar to ours. Nevertheless, it is difficult to identify the reasons for this as no details regarding the size of the cluster or scattering potential are given in Ref. 4. Note, however, that angular momentum projected densities of both occupied and unoccupied states of TiS_2 calculated recently by a

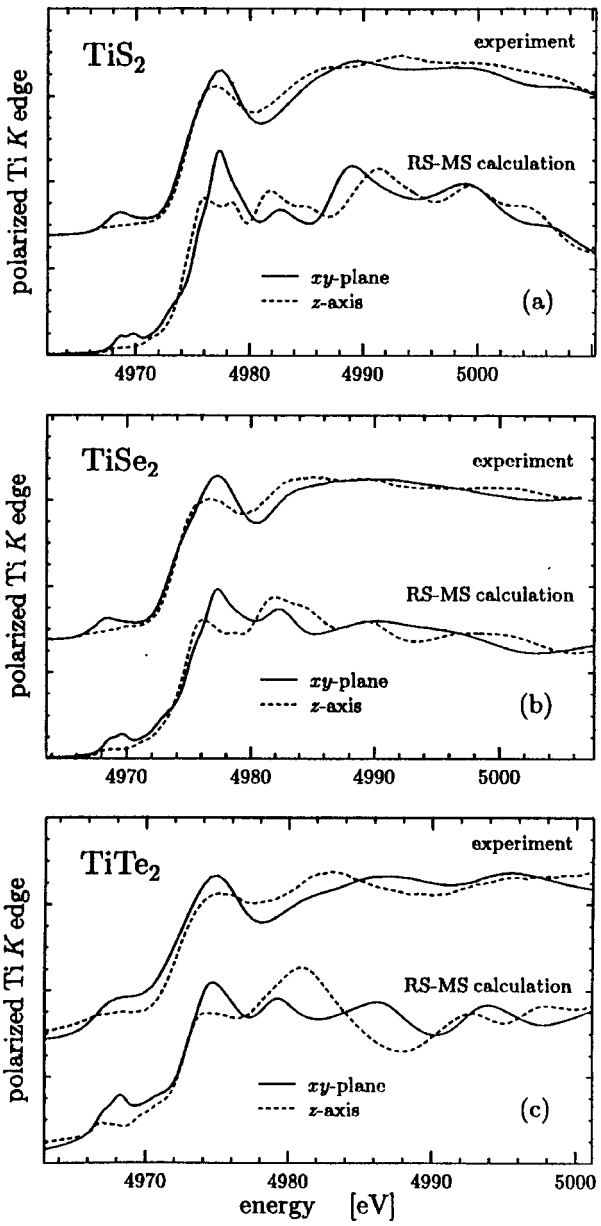

FIG. 6. Experimental and theoretical polarized Ti *K*-edge spectra of (a) TiS_2, (b) $TiSe_2$, and (c) $TiTe_2$ within equivalent energy ranges obtained by extending the energy scale by the scaling factors of Table II. Experimental curves represent averages of several polarization decompositions (or partial spectral components) as shown in Figs. 3(b), 4(b), and 5(b). Theoretical curves are the results of real-space multiple-scattering calculations for clusters of 135 atoms. A broadening by an energy-dependent Lorentzian to account for the core hole lifetime and inelastic photoelectron losses was included.

pseudopotential method[7] or by a full-potential linearized augmented-plane-wave method[20] disagree with the results presented by Antonangeli *et al.*[4] as well.

The prepeak at 4968 eV in Ti *K*-edge spectra of titanium dichalcogenides[6,7] and related compounds[21] has been the subject of an intensive study. Our analysis clearly demonstrates that the quadrupole contribution to this prepeak is negligible for all three investigated compounds. Otherwise, one would never reach such a good coincidence in the polarization decomposition performed for different ''sets'' of spectra, taking into account the dipole $1s$-p transitions only

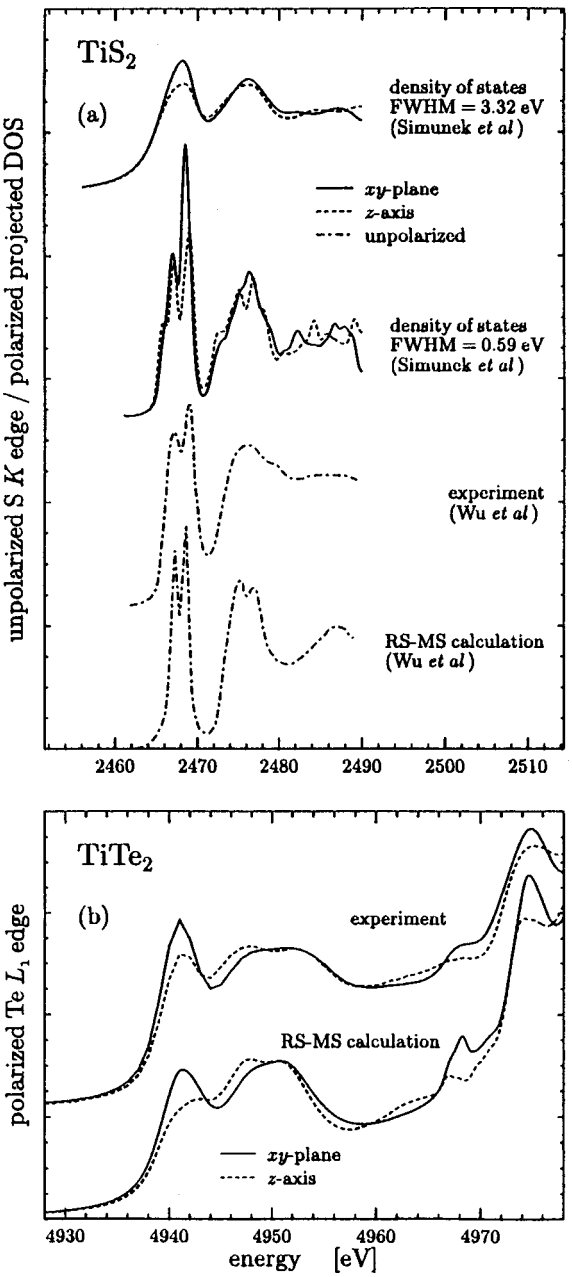

FIG. 7. (a) Experimental and theoretical unpolarized S *K*-edge spectra of TiS_2 (from Ref. 5) and partial DOS (from Ref. 7) together with (b) the measured and calculated polarized Te L_1-edge spectra of $TiTe_2$ within equivalent energy ranges. The DOS is displayed broaden by a Lorentzian with a FWHM of 3.32 eV (upper curves) and 0.59 eV (lower curves). The experimental spectra of $TiTe_2$ represent averages of two polarization decompositions (or partial spectral components) as shown in Fig. 5(b). The theoretical curves for the $TiTe_2$ spectrum are a result of a real-space multiple-scattering calculation for a cluster of 138 atoms. A broadening by an energy-dependent Lorentzian to account for the core hole lifetime and inelastic photoelectron losses was included.

(Figs. 3–5). Hence any participation of the Ti $3d$ states in this transition can arise only through $3d$-$4p$ hybridization.

The double structure of the prepeak, predicted by the theory[6,7] for TiS_2, appears in $TiSe_2$ and $TiTe_2$ theoretical curves as well. These two subpeaks are not fully resolved in the experimental spectra; nevertheless, there is clear evidence that there is a complex structure involved (Figs. 3–6). Regarding the polarization dependence of the prepeak, Šimůnek *et al.*[7] argue on basis of self-consistent electronic structure calculations that in TiS_2 the first subpeak appears in the $p_{x,y}$ polarization only, while the second one is isotropic. Our experimental data for $TiSe_2$ and $TiTe_2$ suggest that this conclusion might be valid for the other two layered dichalcogenides as well.

The largest discrepancy between the theoretical and experimental curves occurs within the region above the main peak for all three compounds (in the region 4980–4985 eV). The occurrence of a redundant structure at this energy seems to be a general drawback of all calculations: for TiS_2, it appears in the RS-MS results of Wu *et al.*[6] as well as in self-consistent band-structure calculations of Šimůnek *et al.*[7]

The disagreement is most prominent for the p_z component in TiS_2, where it is hardly possible to find any experimental counterpart to the theoretical peak at 4982 eV. Interestingly, the same feature, which is apparently redundant in TiS_2, appears both in the calculated and, less pronounced but still distinct, in the experimental spectrum of $TiSe_2$. Hence there seems to be a sufficient reason to believe that the suppression of the fine structure around 4981–4983 eV in TiS_2 is a many-body effect and that this effect is not the same in TiS_2 and in $TiSe_2$. The simple linearly energy-dependent Lorentzian broadening clearly is not good enough to account for this fact.

The Te L_1-edge polarized spectrum of $TiTe_2$ is compared with the unpolarized S *K*-edge spectrum of TiS_2 in Fig. 7. The energy range available for comparing the two spectra is quite small in comparison to the Ti *K* spectra in Fig. 6. As a consequence, one cannot judge unambiguously whether or not there is an overall similarity between the TiS_2 and $TiTe_2$ anion spectra. The spectra resemble each other in the beginning: The separation between the first peak at 2468 eV (TiS_2) or 4941 eV ($TiTe_2$) and the second one (at 2476 eV for TiS_2 and 4947 eV for $TiTe_2$) is very similar in both compounds, provided the energy scaling of Eq. (6) is taken into account (cf Fig. 7). Also the polarization dependence of the Te L_1 edge in $TiTe_2$ is the same as the computed polarization dependence of the S *K* edge in TiS_2,[7] i.e., the first peak is higher for the $p_{x,y}$ polarization than for the p_z symmetry, while the second peak is more or less isotropic. This polarization feature ought to persist at the Te edge as well: We display in Fig. 7 the polarized densities of states broaden by a Lorentzian with a full width at half maximum (FWHM) equal to both 0.59 eV (lower curves, corresponding to the S *K* edge) and 3.32 eV (upper curves, corresponding to the Te L_1 edge). On the other hand, the third peaks (at 2487 eV for TiS_2 and at 4952 eV for $TiTe_2$) differ in their positions quite a lot so they do not seem to be analogous to one another.

The first peak is distinctly split in TiS_2 both in the experiment and in the theory:[5,7] The separation of sub-peaks is 2 eV. A similar splitting occurs in our RS-MS calculation for $TiTe_2$ for very large cluster sizes (more than 60 atoms) as well and the same is true also for projected Te *p* density of states derived from the self-consistent band-structure calculation of Claessen *et al.*[3] However, due to different core hole widths (3.32 eV for the Te $2s$ level compared to 0.59 eV for the S $1s$ level[17]), such a splitting cannot be present in the $TiTe_2$ experimental spectrum.

A not-so-perfect coincidence between the experimental

polarized curves extracted from different data sets at Te L_1 absorption edge (cf. Fig. 5) could be caused by experimental errors or (less probably) may indicate the presence of a nonnegligible quadrupole contribution. The fact that there is less of a correspondence between anion edges than between cation ones is not surprising: When comparing cation edges (Fig. 6), the absorbing atom is always the same, viz., titanium, while it changes from S to Te for anion edges (Fig. 7). Hence it is natural to expect that the differences in electronic structure would have a better chance to get revealed through anion edges than through cation ones.

VII. CONCLUSIONS

The results of the comparative analysis of the three titanium dichalcogenides could be summarized in the following points. The main spectral peaks and polarization features in x-ray-absorption spectra of TiS_2, $TiSe_2$, and $TiTe_2$ can be reproduced by a real-space multiple-scattering calculation within a one-electron theory. The good agreement between polarized spectra obtained from different data sets as well as between the experimental and the theoretical curves for each compound demonstrate the suitability and usefulness of our procedure for the polarization decomposing.

The Ti *K*-edge spectra of all three compounds are qualitatively quite similar to each other, especially if the differences in lattice constants are diminished by comparing them in the equivalent energy scales. This is really true for the trends in polarization dependence, in particular in the case of the prepeak. Some quantitative differences between spectra of different compounds still persist after the scaling, thus manifesting differences in the electronic structure. Specifically there is evidence that many-body effects underlying photoelectron inelastic energy losses are different in TiS_2 and $TiSe_2$ and are responsible for suppression of the fine structure between 4980 and 4985 eV in Ti *K*-edge XANES of TiS_2.

As far as the Te L_1-edge spectrum of $TiTe_2$ and the S *K*-edge spectrum of TiS_2 are concerned, again some similarities between them can be seen. However, clear differences between them persist even after energy scaling, especially beyond the absorption edge.

ACKNOWLEDGMENTS

The experimental work was supported by the Hamburger Synchrotronstrahlungslabor HASYLAB (Project No. II-95-67). The theoretical work was supported by Grant No. A 1010608 of the Academy of Sciences of the Czech Republic and Grant No. 202/97/0566 of the Grant Agency of the Czech Republic. The use of the CRYSTIN crystallographic database was supported by Project No. 203/96/0111 of the Grant Agency of the Czech Republic.

[1] C. M. Fang, R. A. de Groot, and C. Haas, Phys. Rev. B **56**, 4455 (1997).
[2] A. Bodicker and W. Schattke, Phys. Rev. B **55**, 5045 (1997).
[3] R. Claessen, R. O. Anderson, G.-H. Gweon, J. W. Allen, W. P. Ellis, C. Janowitz, C. G. Olson, Z. X. Shen, V. Eyert, M. Skibowski, K. Friemelt, E. Bucher, and S. Hufner, Phys. Rev. B **54**, 2453 (1996).
[4] F. Antonangeli, M. Piacentini, R. Girlanda, G. Martino, and E. S. Giuliano, Phys. Rev. B **32**, 6644 (1983).
[5] Z. Y. Wu, F. Lemoigno, P. Gressier, G. Ouvrard, P. Moreau, J. Rouxel, and C. R. Natoli, Phys. Rev. B **54**, R11 009 (1996).
[6] Z. Y. Wu, G. Ouvrard, P. Moreau, and C. R. Natoli, Phys. Rev. B **55**, 9508 (1997).
[7] A. Šimůnek, O. Šipr, S. Bocharov, D. Heumann, and G. Dräger, Phys. Rev. B **56**, 12 232 (1997).
[8] Z. Y. Wu, G. Ouvrard, S. Lemaux, P. Moreau, P. Gressier, F. Lemoigno, and J. Rouxel, Phys. Rev. Lett. **77**, 2101 (1996).
[9] G. Dräger, R. Frahm, G. Materlik, and O. Brüemmer, Phys. Status Solidi B **146**, 287 (1988).
[10] D. Heumann, D. Hofmann, and G. Dräger, Physica B **208&299**, 305 (1995).
[11] P. J. Durham, in *X-Ray Absorption*, edited by D. C. Kronigsberger and R. Prins (Wiley, New York, 1988), p. 53; D. D. Vvedensky, in *Unoccupied Electronic States*, edited by J. C. Fuggle and J. E. Inglesfield (Springer-Verlag, Berlin, 1992), p. 139.
[12] D. D. Vvedensky, D. K. Saldin, and J. B. Pendry, Comput. Phys. Commun. **40**, 421 (1986).
[13] W. Kohn and L. J. Sham, Phys. Rev. **140**, A1133 (1965).
[14] G. Bergerhoff, R. Hundt, R. Sievers, and I. D. Brown, J. Chem. Inform. Comput. Sci. **23**, 66 (1983).
[15] B. W. Holland, J. B. Pendry, R. F. Pettifer, and J. Bordas, J. Phys. C **11**, 633 (1978); R. V. Vedrinskii, L. A. Bugaev, and V. M. Airapetian, J. Phys. B **24**, 1967 (1991).
[16] O. Šipr, P. Machek, A. Šimůnek, J. Vackar, and J. Horak, Phys. Rev. B **56**, 13 151 (1997).
[17] F. Al Shamma, M. Abbate, and J. C. Fuggle, in *Unoccupied Electronic States* (Ref. 11), p. 348.
[18] W. Speier, R. Zeller, and J. Fuggle, Phys. Rev. B **32**, 3597 (1985).
[19] M. T. Czyzyk, R. A. de Groot, G. Dalba, P. Fornasini, A. Kisiel, F. Rocca, and E. Burattini, Phys. Rev. B **39**, 9831 (1989).
[20] A. Šimůnek and F. Máca (unpublished).
[21] Z. Y. Wu, G. Ouvrard, P. Gressier, and C. R. Natoli, Phys. Rev. B **55**, 10 382 (1997).
[22] C. Brouder, J. Phys. C **2**, 701 (1990).